Supporting Information for "On the existence of multiple states of low flow regimes in catchments in southeast Australia"

Pallavi Goswami[1], Tim J. Peterson[2,3], Arpita Mondal[4,5], Christoph Rüdiger[2,6]

[1]IITB-Monash Research Academy, IIT Bombay, Mumbai, India
[2]Department of Civil Engineering, Monash University, Clayton, Victoria, Australia
[3]Department of Infrastructure Engineering, University of Melbourne, Parkville, Victoria, Australia
[4]Department of Civil Engineering, Indian Institute of Technology Bombay, Mumbai, India
[5]Interdisciplinary Program in Climate Studies, Indian Institute of Technology Bombay, Mumbai, India
[6]Bureau of Meteorology, Melbourne, Victoria, Australia

Introduction

This document contains text, figures, and tables that are meant to provide additional details that supplements some of the information provided in the Methods and Results & Discussion sections of the paper to which this SI is associated.

Contents of this file:

1. Text S1–S5
2. Tables S1–S3
3. Figures S1–S6

Corresponding author: Pallavi Goswami, IITB-Monash Research Academy, IIT Bombay, Mumbai, Maharashtra 400076, India. (Pallavi.Goswami@monash.edu)

Text S1. Details of the streamflow gauge stations

Table S1, adopted from Supplementary Information of Goswami et al. (2022), details information on the gauges used for the study. The streamflow data was taken from Peterson et al. (2021), wherein all the gauges used were quality controlled. Monthly streamflow data as flow depth (in mm) are available for these catchments, obtained by aggregating daily data. The area of these catchments ranges from 5.5 to 8463.6 km^2, with a median catchment area of 295.6 km^2. For more details, the reader is referred to the Supplementary Material of Peterson et al. (2021). The streamflow data used for this study, along with the catchment shapefiles, are available at `https://zenodo.org/record/6659706#.Y52tpHZBxdg`. Table S1 is followed by Table S2, displaying the overall mean and median values of flow depth for all these catchments taken together.

Table S1: Details of the streamflow gauge stations used in the study

Sr. No.	Gauge ID	Gauge name	Catchment area (km^2)	Latitude (°S)	Longitude (°E)	Data starting from	Data up to	No. of months for which data was unavailable	Years of available data
1	221201	CANN RIVER (WEST BRANCH) WEERAGUA	323.30	37.37	149.2	May 1922	Jul 2017	271	72.67
2	221207	ERRINUNDRA RIVER ERRINUNDRA	160.88	37.45	148.92	Apr 1968	Jul 2017	7	48.83
3	221208	WINGAN RIVER WINGAN INLET NATIONAL PARK	419.83	37.69	149.49	Sep 1979	Jul 2017	0	38.08
4	221209	CANN RIVER (EAST BRANCH) WEERAGUA	148.09	37.36	149.21	Feb 1973	Jul 2017	3	44.5
5	221210	GENOA RIVER THE GORGE	836.84	37.42	149.52	Jan 1973	Jul 2017	0	44.92
6	221211	COMBIENBAR RIVER COMBIENBAR	178.54	37.44	148.98	Feb 1975	Jul 2017	0	42.92
7	221212	BEMM RIVER PRINCES HIGHWAY	730.62	37.61	148.9	Nov 1975	Jul 2017	4	41.92
8	222202	BRODRIBB RIVER SARDINE CREEK	650.16	37.51	148.55	Dec 1922	Aug 2017	198	78.83
9	222206	BUCHAN RIVER BUCHAN	847.74	37.5	148.17	Dec 1926	Aug 2017	206	74.25
10	222210	DEDDICK RIVER DEDDICK (CASEYS)	847.70	37.09	148.42	Jan 1965	Aug 2017	47	49.5
11	222217	RODGER RIVER JACKSONS CROSSING	433.18	37.41	148.36	Apr 1977	Aug 2017	0	41.25
12	223202	TAMBO RIVER SWIFTS CREEK	896.08	37.27	147.73	May 1948	Jul 2017	1	70.08
13	223204	NICHOLSON RIVER DEPTFORD	289.37	37.59	147.7	Jun 1962	Jul 2017	7	55.58
14	223205	TAMBO RIVER D/S OF RAMROD CREEK	2676.68	37.67	147.87	Aug 1966	Jul 2017	0	52.08
15	224201	WONNANGATTA RIVER WATERFORD	1974.27	37.49	147.17	Jun 1923	Jul 2017	292	71
16	224203	MITCHELL RIVER GLENALADALE	3920.57	37.76	147.37	Dec 1938	Jul 2017	0	79.92
17	224206	WONNANGATTA RIVER CROOKED RIVER	1103.33	37.41	147.09	Oct 1954	Jul 2017	4	63.83
18	224213	DARGO RIVER LOWER DARGO ROAD	668.17	37.5	147.27	Nov 1974	Jul 2017	2	44
19	224214	WENTWORTH RIVER TABBERABBERA	440.75	37.5	147.39	Feb 1976	Jul 2017	3	42.75
20	225201	AVON RIVER STRATFORD	1467.28	37.97	147.08	Jul 1978	Jul 2017	0	40.67
21	225209	MACALISTER RIVER LICOLA	1237.60	37.63	146.62	Apr 1954	Jul 2017	9	64.25
22	225213	ABERFELDY RIVER BEARDMORE	312.39	37.85	146.43	Apr 1965	Aug 2017	1	54.08
23	225218	FREESTONE CREEK BRIAGALONG	304.99	37.81	147.1	Mar 1969	Aug 2017	0	50.33
24	225219	MACALISTER RIVER GLENCAIRN	572.36	37.52	146.57	Apr 1969	Jul 2017	2	50.08
25	225221	MACALISTER RIVER STRINGYBARK CREEK	1542.29	37.77	146.67	Apr 1970	Aug 2017	54	44.92
26	225223	VALENCIA CREEK GILLIO ROAD	203.19	37.74	146.99	Nov 1973	Aug 2017	19	44.33
27	225224	AVON RIVER THE CHANNEL	557.42	37.8	146.88	Oct 1974	Aug 2017	1	45
28	226023	TRARALGON CREEK TRARALGON	172.40	38.19	146.54	Feb 1963	Jul 2017	72	50.75
29	226204	LATROBE RIVER WILLOW GROVE	560.91	38.09	146.16	Mar 1927	Aug 2017	0	92.83
30	226205	LATROBE RIVER NOOJEE	295.57	37.91	146.02	Sep 1959	Jul 2017	3	60.08
31	226209	MOE RIVER DARNUM	230.59	38.21	146	Feb 1964	Aug 2017	0	56.08
32	226218	NARRACAN CREEK THORPDALE	65.73	38.27	146.19	Feb 1958	Aug 2017	0	62.17
33	226220	LOCH RIVER NOOJEE	106.01	37.87	146.01	Dec 1959	Jul 2017	37	57.25
34	226226	TANJIL RIVER TANJIL JUNCTION	297.73	37.98	146.19	Mar 1963	Aug 2017	1	57.17
35	226402	MOE DRAIN TRAFALGAR EAST	610.47	38.18	146.21	May 1960	Aug 2017	0	60.17
36	226407	MORWELL RIVER BOOLARRA	116.51	38.41	146.31	Oct 1961	Aug 2017	120	48.83
37	227200	TARRA RIVER YARRAM	217.08	38.54	146.67	Mar 1949	Jul 2017	18	69.92
38	227202	TARWIN RIVER MEENIYAN	1072.24	38.58	145.99	Aug 1958	Aug 2017	0	62.17
39	227205	MERRIMAN CREEK CALIGNEE SOUTH	39.48	38.35	146.65	Mar 1950	Aug 2017	189	54.92
40	227210	BRUTHEN CREEK CARRAJUNG LOWER	17.91	38.4	146.74	Dec 1955	Jul 2017	0	64.92
41	227211	AGNES RIVER TOORA	66.09	38.64	146.37	May 1956	Aug 2017	45	60.92
42	227213	JACK RIVER JACK RIVER	34.88	38.53	146.54	Mar 1964	Jul 2017	0	56.83
43	227219	BASS RIVER LOCH	53.31	38.36	145.73	Oct 1969	Jul 2017	2	51.17
44	227225	TARRA RIVER FISCHERS	19.00	38.47	146.56	Dec 1971	Jul 2017	2	49.08
45	227226	TARWIN RIVER EAST BRANCH DUMBALK NORTH	125.64	38.5	146.16	Jan 1974	Aug 2017	0	47.33
46	227227	WILKUR CREEK LEONGATHA	105.28	38.39	145.96	May 1974	Jul 2017	0	47
47	227236	POWLETT RIVER D/S FOSTER CREEK JUNCTION	233.33	38.56	145.71	Apr 1983	Jul 2017	1	38.08
48	227237	FRANKLIN RIVER TOORA	75.23	38.63	146.31	Jun 1983	Aug 2017	0	38.17
49	230205	DEEP CREEK BULLA (D/S OF EMU CREEK JUNCT.)	865.25	37.63	144.8	Jul 1959	Aug 2017	5	61.75
50	230209	BARRINGO CREEK BARRINGO (U/S OF DIVERSION)	5.53	37.41	144.63	Aug 1970	Aug 2017	1	51.08

Sr. No.	Gauge ID	Gauge name	Catchment area (km^2)	Latitude (°S)	Longitude (°E)	Data starting from	Data up to	No. of months for which data was unavailable	Years of available data
51	230210	SALTWATER CREEK BULLENGAROOK	38.91	37.47	144.52	Aug 1972	Aug 2017	2	49.08
52	231225	WERRIBEE RIVER BALLAN (U/S OLD WESTERN HWY)	107.49	37.6	144.25	Sep 1977	Aug 2017	1	44.17
53	231231	TOOLERN CREEK MELTON SOUTH	94.53	37.73	144.58	Sep 1983	Dec 2015	0	36.67
54	232214	BLACK CREEK U/S OF BUNGAL DAM	12.78	37.63	144.06	Dec 1981	Aug 2017	2	40
55	232215	WOOLLEN CREEK U/S OF BUNGAL DAM	8.62	37.63	144.08	Jan 1982	Aug 2017	0	40.17
56	233211	BIRREGURRA CREEK RICKETTS MARSH	114.29	38.3	143.84	Feb 1958	Aug 2017	14	63
57	233214	BARWON RIVER EAST BRANCH FORREST	16.59	38.53	143.73	Feb 1960	Aug 2017	0	62.25
58	233223	WARRAMBINE CREEK WARRAMBINE	53.87	37.93	143.87	Mar 1975	Aug 2017	1	47.17
59	234200	WOADY YALOAK RIVER PITFIELD	315.32	37.81	143.59	Jun 1922	Aug 2017	355	70.5
60	234201	WOADY YALOAK RIVER CRESSY (YARIMA)	1155.17	38.01	143.64	May 1960	Aug 2017	7	61.67
61	234203	PIRRON YALLOCK CREEK PIRRON YALLOCK (ABOVE H'WY BR.)	169.11	38.35	143.42	May 1969	Jul 2017	0	53.25
62	234209	DEAN CREEK LAKE COLAC	53.12	38.34	143.56	Jan 1981	Aug 2017	0	41.75
63	235203	CURDIES RIVER CURDIE	781.68	38.44	142.96	Jan 1961	Jul 2017	3	61.5
64	235204	LITTLE AIRE CREEK BEECH FOREST	11.17	38.65	143.53	Aug 1960	Aug 2017	70	56.5
65	235209	AIRE RIVER BEECH FOREST	25.22	38.67	143.58	Aug 1969	Aug 2017	0	53.42
66	235210	LARDNER CREEK GELLIBRAND	51.74	38.53	143.54	Dec 1969	Aug 2017	4	52.83
67	235211	KENNEDYS CREEK KENNEDYS CREEK	269.42	38.59	143.26	Jan 1970	Aug 2017	7	52.58
68	235216	CUMBERLAND RIVER LORNE	38.19	38.57	143.95	Dec 1971	Aug 2017	0	51.33
69	235219	AIRE RIVER WYELANGTA	91.16	38.7	143.48	Dec 1972	Aug 2017	3	50.17
70	235227	GELLIBRAND RIVER BUNKERS HILL	313.65	38.52	143.48	Jan 1976	Aug 2017	8	46.75
71	235233	BARHAM RIVER EAST BRANCH APOLLO BAY PARADISE	43.45	38.76	143.62	Sep 1983	Aug 2017	1	39.75
72	235234	LOVE CREEK GELLIBRAND	76.66	38.48	143.57	Apr 1985	Aug 2017	0	38.33
73	236202	HOPKINS RIVER WICKLIFFE	1358.79	37.7	142.72	Jun 1970	Aug 2017	4	52.92
74	236203	MOUNT EMU CREEK SKIPTON	1230.00	37.69	143.36	Aug 1926	Aug 2017	142	85.33
75	236204	FIERY CREEK STREATHAM	1001.32	37.68	143.06	Sep 1926	Aug 2017	123	86.92
76	236205	MERRI RIVER WOODFORD	888.01	38.32	142.48	Nov 1954	Jul 2017	3	68.75
77	236209	HOPKINS RIVER HOPKINS FALLS	8463.59	38.34	142.63	Oct 1961	Jul 2017	3	61.92
78	236210	HOPKINS RIVER FRAMLINGHAM	5143.99	38.24	142.7	Dec 1961	Jul 2017	0	62.08
79	236212	BRUCKNELL CREEK CUDGEE	230.51	38.35	142.65	Jan 1972	Jul 2017	0	52.08
80	236213	MOUNT EMU CREEK MENA PARK	313.91	37.53	143.46	Aug 1973	Aug 2017	2	50.5
81	236216	MOUNT EMU CREEK TAROON (AYRFORD ROAD BRIDGE)	2946.43	38.31	142.88	Jul 1984	Jul 2017	5	39.33
82	237200	MOYNE RIVER TOOLONG	568.69	38.32	142.23	Mar 1955	Jul 2017	0	69.17
83	237202	FITZROY RIVER HEYWOOD	264.11	38.13	141.62	Jun 1955	Aug 2017	0	69.08
84	237205	DARLOT CREEK HOMERTON BRIDGE	748.34	38.15	141.77	Jan 1970	Aug 2017	0	54.58
85	237206	EUMERALLA RIVER CODRINGTON	458.01	38.26	141.94	Mar 1971	Aug 2017	0	53.5
86	237207	SURRY RIVER HEATHMERE	296.06	38.24	141.66	Jun 1977	Aug 2017	0	47.33
87	238208	JIMMY CREEK JIMMY CREEK	22.24	37.37	142.51	Apr 1957	Aug 2017	0	67.58
88	238219	GRANGE BURN MORGIANA	1110.91	37.71	141.83	Nov 1970	Jul 2017	55	49.42
89	238223	WANDO RIVER WANDO VALE	173.58	37.5	141.43	Sep 1971	Aug 2017	2	53.17
90	238229	CHETWYND RIVER CHETWYND	69.75	37.32	141.48	Sep 1974	Jun 2017	7	49.67
91	238230	STOKES RIVER TEAKETTLE	191.46	37.87	141.41	Jan 1974	Aug 2017	3	50.92
92	238235	CRAWFORD RIVER LOWER CRAWFORD	613.62	37.98	141.45	Jan 1978	Aug 2017	0	47.25
93	401203	MITTA MITTA RIVER HINNOMUNJIE	1531.39	36.95	147.61	Mar 1933	Jul 2017	2	91.92
94	401208	CUDGEWA CREEK BERRINGAMA	357.52	36.21	147.68	Feb 1961	Aug 2017	0	64.33
95	401210	SNOWY CREEK BELOW GRANITE FLAT	413.32	36.57	147.41	Sep 1940	Aug 2017	0	84.83
96	401212	NARIEL CREEK UPPER NARIEL	255.72	36.45	147.83	Apr 1962	Aug 2017	0	63.33
97	401215	MORASS CREEK UPLANDS	536.17	36.87	147.7	Nov 1937	Jul 2017	1	87.67
98	401216	BIG RIVER JOKERS CREEK	357.48	36.93	147.47	Oct 1942	Jul 2017	3	82.67
99	401217	GIBBO RIVER GIBBO PARK	389.34	36.76	147.71	Oct 1979	Jul 2017	0	46
100	401220	TALLANGATTA CREEK McCALLUMS	454.44	36.21	147.34	Nov 1985	Aug 2017	2	39.92
101	402204	YACKANDANDAH CREEK OSBORNES FLAT	275.16	36.3	146.91	Mar 1973	Aug 2017	3	52.58
102	402206	RUNNING CREEK RUNNING CREEK	127.52	36.54	147.04	Oct 1974	Aug 2017	5	50.92
103	402213	KINCHINGTON CREEK OSBORNES FLAT	120.28	36.32	146.89	Nov 1977	Jul 2017	8	47.58
104	403200	OVENS RIVER WANGARATTA	5119.74	36.35	146.32	Feb 1894	Aug 2017	14	131
105	403205	OVENS RIVERS BRIGHT	493.67	36.73	146.95	Sep 1933	Aug 2017	128	82
106	403209	REEDY CREEK WANGARATTA NORTH	389.38	36.33	146.34	Mar 1949	Aug 2017	1	77.17
107	403213	FIFTEEN MILE CREEK GRETA SOUTH	226.77	36.62	146.24	Nov 1967	Aug 2017	6	58.17
108	403214	HAPPY VALLEY CREEK ROSEWHITE	139.81	36.58	146.82	Jun 1970	Aug 2017	2	56
109	403217	ROSE RIVER MATONG NORTH	178.61	36.82	146.58	Sep 1971	Aug 2017	7	54.42
110	403221	REEDY CREEK WOOLSHED	211.47	36.31	146.6	Jan 1974	Aug 2017	2	52.58
111	403222	BUFFALO RIVER ABBEYARD	415.09	36.91	146.7	Sep 1974	Aug 2017	3	51.92
112	403223	KING RIVER DOCKER ROAD BRIDGE	1085.31	36.52	146.39	May 1975	Aug 2017	3	51.33
113	403224	HURDLE CREEK BOBINAWARRAH	156.03	36.51	146.45	Sep 1975	Aug 2017	0	51.33
114	403226	BOGGY CREEK ANGLESIDE	109.19	36.61	146.36	Aug 1976	Aug 2017	18	49
115	403230	OVENS RIVER ROCKY POINT	2970.15	36.53	146.67	Jan 1975	Aug 2017	4	51.83
116	403232	MORSES CREEK WANDILIGONG	126.02	36.75	146.98	Jul 1982	Aug 2017	10	43.92
117	403233	BUCKLAND RIVER HARRIS LANE	457.07	36.72	146.88	Feb 1982	Aug 2017	6	44.75
118	404204	BOOSEY CREEK TUNGAMAH	830.67	36.12	145.83	Sep 1976	Aug 2017	0	50.75
119	404207	HOLLAND CREEK KELFEERA	460.78	36.61	146.06	Apr 1970	Aug 2017	1	57.17
120	405205	MURRINDINDI RIVER MURRINDINDI ABOVE COLWELLS	107.70	37.41	145.56	Jun 1949	Jul 2017	3	77.83
121	405209	ACHERON RIVER TAGGERTY	626.25	37.32	145.71	Jan 1956	Jul 2017	1	71.5
122	405214	DELATITE RIVER TONGA BRIDGE	358.12	37.16	146.11	Apr 1957	Aug 2017	0	70.5
123	405215	HOWQUA RIVER GLAN ESK	368.65	37.23	146.21	May 1957	Aug 2017	224	51.83
124	405217	YEA RIVER DEVLINS BRIDGE	361.53	37.38	145.47	Jul 1964	Jul 2017	4	63
125	405218	JAMIESON RIVER GERRANG BRIDGE	367.23	37.29	146.19	Nov 1964	Aug 2017	0	63.17
126	405219	GOULBURN RIVER DOHERTYS	701.64	37.33	146.13	Feb 1965	Aug 2017	8	62.33
127	405226	PRANJIP CREEK MOORILIM	791.16	36.62	145.31	Jul 1968	Jul 2017	0	59.58
128	405227	BIG RIVER JAMIESON	626.51	37.37	146.06	Oct 1968	Aug 2017	0	59.5
129	405228	HUGHES CREEK TARCOMBE ROAD	483.80	36.94	145.29	Jun 1969	Jul 2017	1	58.75
130	405229	WANALTA CREEK WANALTA	106.16	36.63	144.87	Mar 1971	Aug 2017	1	57.17
131	405230	CORNELLA CREEK COLBINABBIN	253.08	36.6	144.8	Apr 1971	Aug 2017	4	56.92
132	405234	SEVEN CREEKS D/S OF POLLY MCQUINN WEIR	154.62	36.89	145.68	Jun 1976	Jul 2017	14	50.92
133	405237	SEVEN CREEKS EUROA TOWNSHIP	347.86	36.73	145.57	Jun 1974	Jul 2017	10	53.33
134	405238	MOLLISON CREEK PYALONG	163.47	37.12	144.86	Jul 1977	Sep 2016	6	49.83
135	405240	SUGARLOAF CREEK ASH BRIDGE	609.80	37.06	145.06	Mar 1984	Aug 2017	15	43.42
136	405245	FORD CREEK MANSFIELD	115.73	37.04	146.05	Sep 1981	Aug 2017	1	47.17
137	405246	CASTLE CREEK ARCADIA	202.72	36.59	145.35	Oct 1981	Jun 2017	32	44.42
138	405248	MAJOR CREEK GRAYTOWN	284.69	36.85	144.91	Oct 1982	Aug 2017	1	46.25
139	405251	BRANKEET CREEK ANCONA	118.78	36.97	145.79	Dec 1982	Aug 2017	2	46.08
140	405264	BIG RIVER D/S OF FRENCHMAN CREEK JUNCTION	331.66	37.52	146.08	Nov 1986	Jun 2017	0	42.25
141	405274	HOME CREEK YARCK	180.80	37.11	145.61	Mar 1989	Jul 2017	0	40.08
142	406208	CAMPASPE RIVER ASHBOURNE	39.05	37.39	144.45	Feb 1945	Aug 2017	0	84.33
143	406213	CAMPASPE RIVER REDESDALE	637.64	37.02	144.54	Sep 1965	Jul 2017	60	58.75
144	406214	AXE CREEK LONGLEA	235.63	36.77	144.43	Mar 1977	Jul 2017	0	52.33
145	406226	MOUNT IDA CREEK DERRINAL	175.63	36.88	144.65	Jul 1990	Jul 2017	2	38.92
146	406235	WILD DUCK CREEK U/S OF HEATHCOTE-MIA MIA ROAD	211.92	36.95	144.66	Jan 1993	Jul 2017	10	35.83
147	407211	BET BET CREEK BET BET	628.62	36.92	143.75	Dec 1955	Jul 2017	350	44.67
148	407214	CRESWICK CREEK CLUNES	310.46	37.3	143.79	Dec 1955	Aug 2017	0	74
149	407217	LODDON RIVER VAUGHAN D/S FRYERS CREEK	295.45	37.16	144.21	Oct 1959	Jul 2017	3	69.92
150	407221	JIM CROW CREEK YANDOIT	166.79	37.21	144.1	Dec 1966	Jul 2017	3	62.83
151	407230	JOYCES CREEK STRATHLEA	149.01	37.16	143.96	Dec 1975	Jul 2017	0	54.17
152	407239	MIDDLE CREEK RODBOROUGH	148.06	37.14	143.91	Jan 1983	Jul 2017	144	35.17
153	407246	BULLOCK CREEK MARONG	188.61	36.73	144.14	Nov 1985	Jul 2017	3	44.17
154	408202	AVOCA RIVER AMPHITHEATRE	76.54	37.18	143.41	Aug 1979	Aug 2017	7	50.25
155	415201	WIMMERA RIVER GLENORCHY WEIR TAIL GAUGE	1967.83	36.91	142.64	Nov 1962	Aug 2017	4	67.33
156	415206	WIMMERA RIVER GLYNWYLLN	1377.05	36.95	142.86	Sep 1915	Aug 2017	504	72.92
157	415207	WIMMERA RIVER EVERSLEY	305.00	37.19	143.18	Nov 1915	Aug 2017	708	55.83
158	415220	AVON RIVER WIMMERA HIGHWAY	519.88	36.64	142.98	Mar 1976	Aug 2017	22	52.75
159	415226	RICHARDSON RIVER CARRS PLAINS	129.91	36.74	142.79	Jul 1984	Aug 2017	7	45.75
160	415237	CONCONGELLA CREEK STAWELL	241.27	37.03	142.82	Apr 1990	Aug 2017	1	40.58
161	415238	WATTLE CREEK NAVARRE	138.75	36.9	143.11	Jul 1989	Aug 2017	11	40.58

Table S2: Median and mean flow depths for the study region taking all catchments into account

	Jan	Feb	Mar	Apr	May	Jun	Jul	Aug	Sep	Oct	Nov	Dec
Median of flow depth (mm)	2.26	1.37	1.36	1.96	3.52	7.95	16.96	24.93	22.79	15.23	7.74	4.27
Mean of flow depth (mm)	6.55	4.90	4.83	6.70	10.77	20.36	32.11	40.24	37.35	29.93	17.86	11.35

Text S2. Box-Cox transformation of streamflows

The flow data for most of the studied catchments was highly skewed towards lower flow values. Since the analysis required deriving a standardized streamflow index, it is important that the series of this standardized streamflow index is as close to a normal distribution as possible. However, with skewed flow data, such an outcome could not be achieved. A Box-cox transformation was thus used to normalize the flow data. The Box-Cox transformation is a power transformation that eliminates non-linearity between variables, differing variances, and variable asymmetry. It is commonly used to transform a series into a new series with an almost normal distribution. Although it is not always possible for a power transformation to bring the distribution to exactly normal, the usual estimates of λ will lead to a distribution that satisfies certain restrictions on the first 4 moments which thus will usually be symmetric. For the present study, a one-parameter Box-Cox transformation of the original streamflow depth data (for $Q_i > 0$) was done, as expressed below.

$$\widehat{Q_i} = (Q_i + 1)^{\lambda} - 1 for \lambda \neq 0 \tag{1}$$

$$\widehat{Q_i} = \ln (Q_i + 1) for \lambda = 0 \tag{2}$$

In the above equation, a value of 1 was added to the original value of Q_i to ensure that the quantity being transformed was always greater than 1 for the transformation to be feasible. Here, λ is the transformation parameter of the transformation and was estimated using the

MASS package available in R, through maximum likelihood estimation. Figure S1 shows the plot of log-likelihood vs lambda for station ID 235204 with the dotted lines indicating the 95% confidence interval for the optimum lambda value. Initially, the optimum value of λ was arrived at by trying values from the set (0.1, 5] at increments of 0.1. However, while using this range it was later realized that allowing λ to take negative values improves the transformation for many catchments. Additionally, positive values beyond 2 were hardly selected. The range was thus revised to be [-2,2].

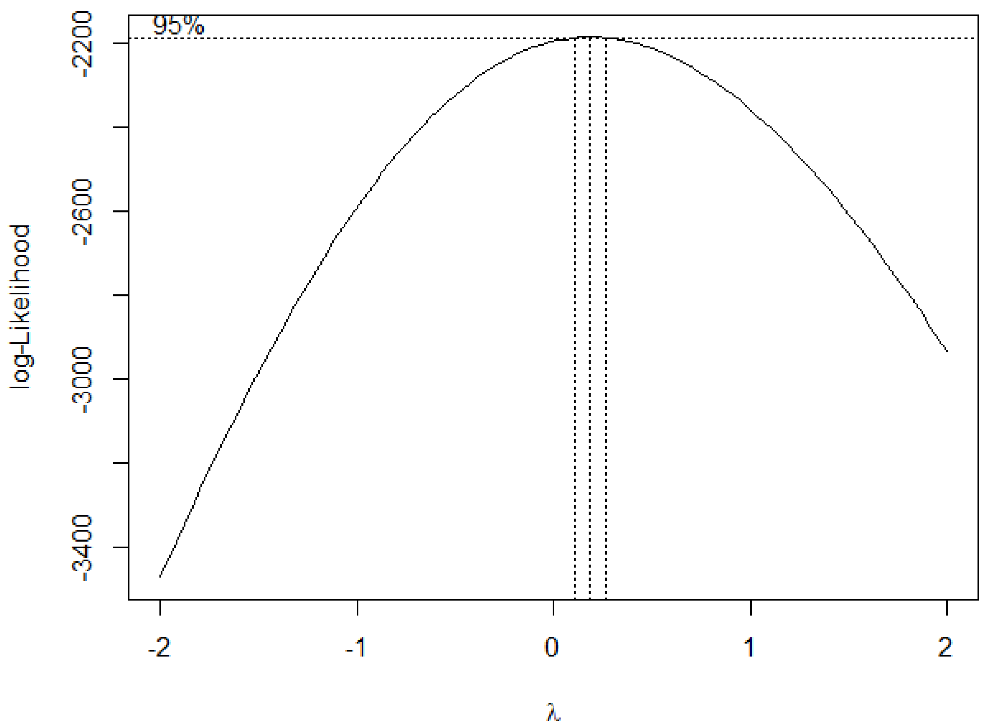

Figure S1: Log-likelihood vs λ for the identification of the optimum value of λ for station ID 235204. The optimization yields a value of $\lambda = 0.18$ as the optimum lambda for the BC transform for this station. The vertical dotted lines around the vertical line at 0.18 indicate the 95% confidence interval for the optimum lambda value.

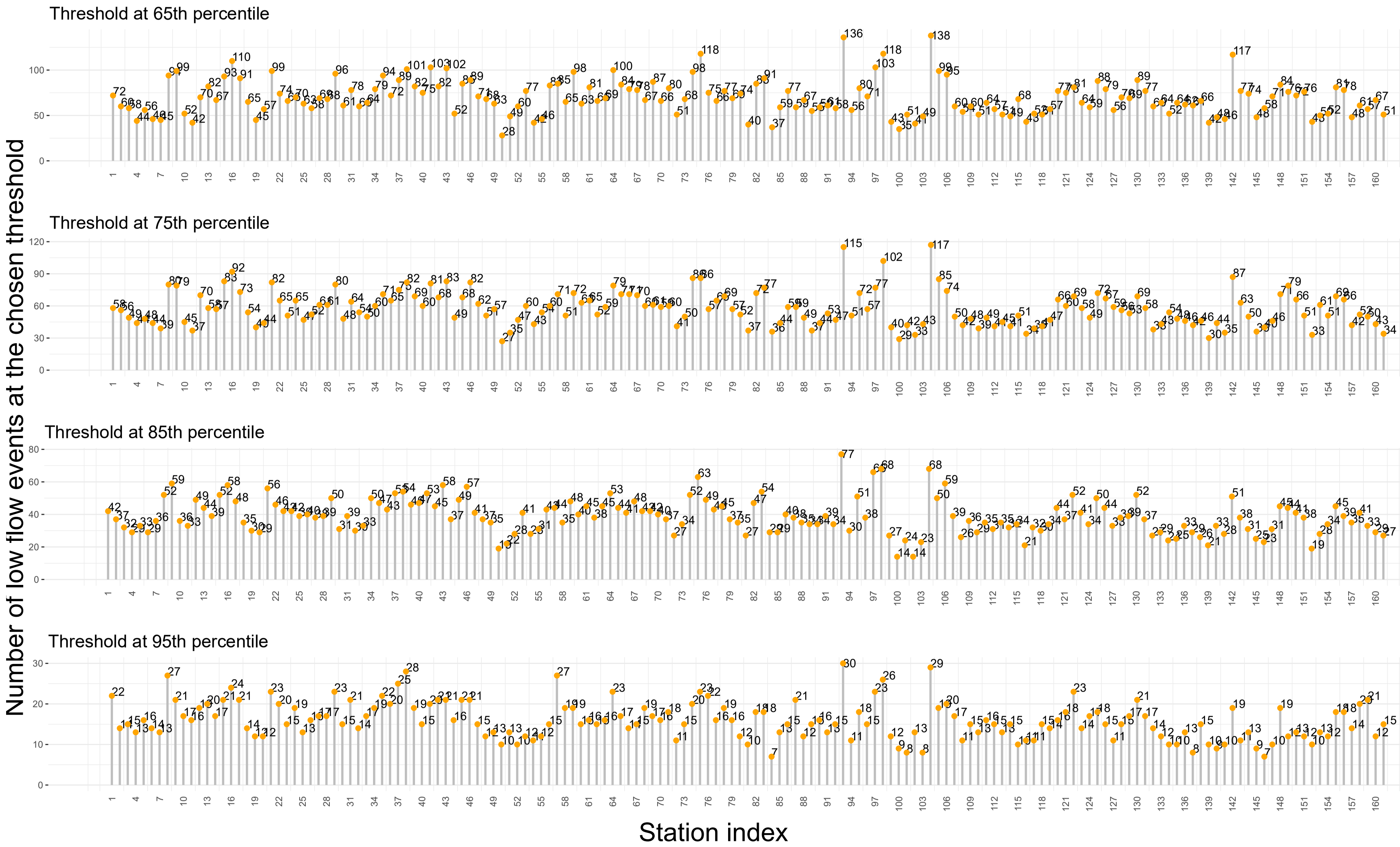

Figure S2: Number of low flow events for each catchment for a chosen value of threshold. From top to bottom, the sub-figures correspond to the 65th, 75th, 85th, and 95th percentiles of the SDI series, respectively, in the adopted POT approach. For the HMM to simulate satisfactorily, it was considered necessary that most of the catchments should have at least 40 observations for low flow IDF. This was achieved for a threshold of 65th percentile which was consequently chosen for the study.

Text S3. Calibration of the HMMs

The parameters of the HMM were arrived at using a constrained maximum likelihood estimation, where the likelihood function $\mathscr{L}_T$ is expressed as:

$$\mathscr{L}_T = \boldsymbol{\delta P}(x_1)\boldsymbol{\Gamma P}(x_2)....\boldsymbol{\Gamma P}(x_T)1' \tag{3}$$

Here $\boldsymbol{\delta}$ is the initial state distribution (Equation 8 in the paper), $\boldsymbol{\Gamma}$ (as $\boldsymbol{\Gamma}_1$ or $\boldsymbol{\Gamma}_2$) is the transition matrix for the relevant model and T is the number of time steps. $\boldsymbol{P}(x)$ is the $m \times m$ diagonal emissions matrix of probabilities for an m-state HMM, obtained from the error distribution model having the ith diagonal element equal to the probability of being in state i at a given point in time (Equation 9,12, or 15 in the paper). The emission probabilities $\boldsymbol{P}$ were obtained from the corresponding error distribution model used to model the variable x.

The likelihood was estimated recursively as $\mathscr{L}_T = \alpha_T 1'$, where

$$\alpha_1 = \boldsymbol{\delta P}(x_1) \tag{4}$$

and

$$\alpha_t = \alpha_{t-1}\boldsymbol{\Gamma P}(x_t) \quad for\ t = 2, 3, 4, ...T$$

Numerically, $\mathscr{L}_T$ was maximized by rearrangement to a negative log-likelihood and minimized using global optimization.

The optimization response surface of a multi-state HMM often tends to have multiple local optima (Supplementary Material of Peterson et al., 2021). To reliably identify the global optima, a Differential Evolution-based global optimization scheme (Storn & Price, 1997) was adopted. This scheme involves transforming a set of parameter vectors, termed as population, into a new parameter vector set at each generation of evolution. The evolution is brought about by perturbing an old parameter vector with the scaled difference of two arbitrarily selected parameter vectors. The new set members thus obtained are more likely to optimize the objective function. To ensure a robust optimization, the population size per parameter was set as 10 as it has been noted that convergence to the global optimum is facilitated if this value is 10 or greater (Price et al., 2006). Higher values in this case incurred undesirably larger computational time without significant improvement in the model fit. Further, the maximum number of generations was set to 550 as nearly all the models were seen to converge at either far less than or near to 550 generations. Model calibration at each catchment was performed 10 times for each state model for the given low flow characteristic. Each calibration was run with a different random seed and a randomly selected differential evolution strategy. To arrive at the most probable sequence of states from all possible combinations of sequences for the given observation sequence of intensity/duration/frequency (I/D/F), an efficient dynamic programming method, called the Viterbi algorithm (Forney, 1973; Zucchini & MacDonald, 2009) was used. This algorithm identifies the most probable sequence of states from the Markov chain of probabilities. The states of I/D/F obtained through this were also referred to as the Viterbi states (named after the algorithm). The algorithm was applied over the entire observation record to identify the most probable sequence of I/D/F states, thereby also identifying any switching, if at all, in the states of the I/D/F.

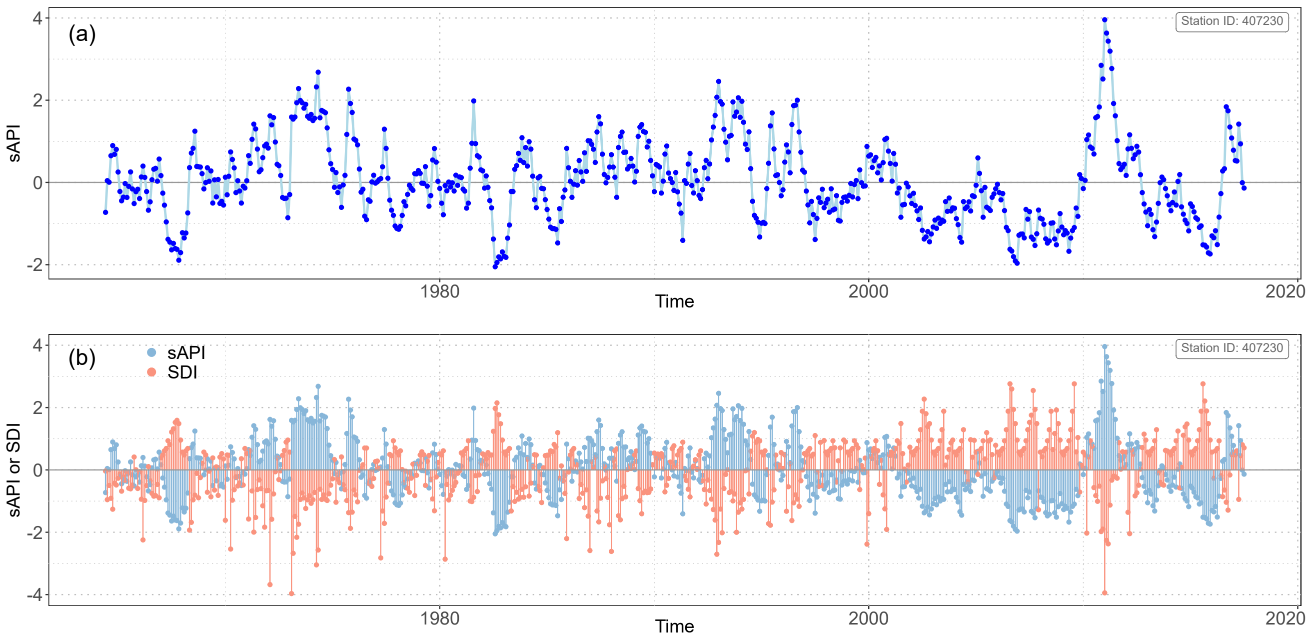

Figure S3: (a) Time series of standardized Antecedent Precipitation Index (sAPI) obtained for station ID 407230. (b) Variation of SDI and sAPI over time for the catchment. The sAPI mirrors the variability in the SDI series of the catchment, making it a suitable choice for a predictor in the HMMs of the low flow characteristics.

Text S4. Assessing model reliability of IDF HMMs through diagnostic plots of residuals

The validity and reliability of the IDF HMMs emerging from the application as discussed in the paper were assessed by inspecting whether the pseudo-residuals were normally distributed or not (Zucchini & MacDonald, 2009). This was carried out by visual inspection of pseudo-residual plots and through the Shapiro-Wilk test (alpha = 0.05) as discussed in the paper under Section 3.1. For models to be accurate, the pseudo-residuals must be normally distributed. The autocorrelation plots of the pseudo-residuals help determine if the model has performed sufficiently well. If minimal autocorrelation is seen to carry into subsequent time steps, it indicates that errors do not accumulate over time and that no information is 'leftover' and not incorporated in the model.

The next three figures represent the assessment of the behavior of residuals of the HMMs of the three low flow characteristic for selected sample stations. Figure S4 gives an example of an acceptable model performance as per the pseudo-residual analysis where the residuals may be considered to be very close to being normally distributed. The auto-correlation of the pseudo-residuals is almost always within the acceptable bounds for many consecutive time steps, indicating that significant information from the data has been included in the model. No or minimal serial correlation of the pseudo-residuals implies that inaccuracies in the model at a given time step have very little effect on future time steps. The Shapiro-Wilk p-value is greater than 0.05 for the pseudo-residuals in Figure S4 which confirms that the residuals are normal and that the model is performing adequately.

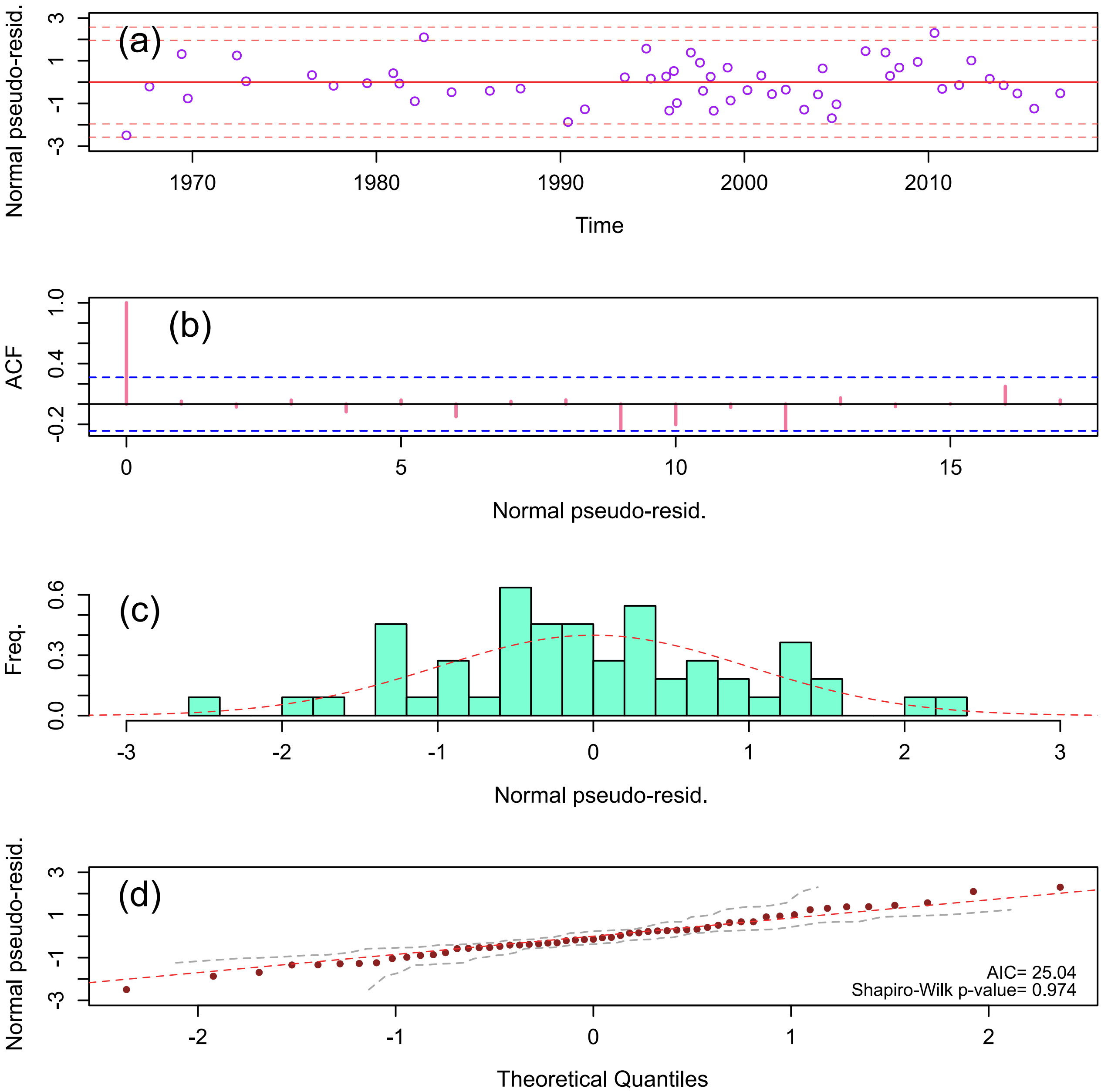

Figure S4: Diagnostic plots of the model residuals corresponding to the intensity HMM output as discussed in Figure 6 for station ID 238223. (a) Time series of the normal pseudo-residuals corresponding to the low flow peaks occurring over time (red lines at 0, ±1.96, ±2.58). (b) Auto-correlation of the normal pseudo-residuals, with the blue dotted lines indicating the 95th percentile confidence intervals for uncorrelated series. (c) Histogram of the normal pseudo-residuals, with the red dotted line indicating a standard normal distribution. (d) Quantile-Quantile (Q-Q) plot of the normal pseudo-residuals in relation to the theoretical quantiles.

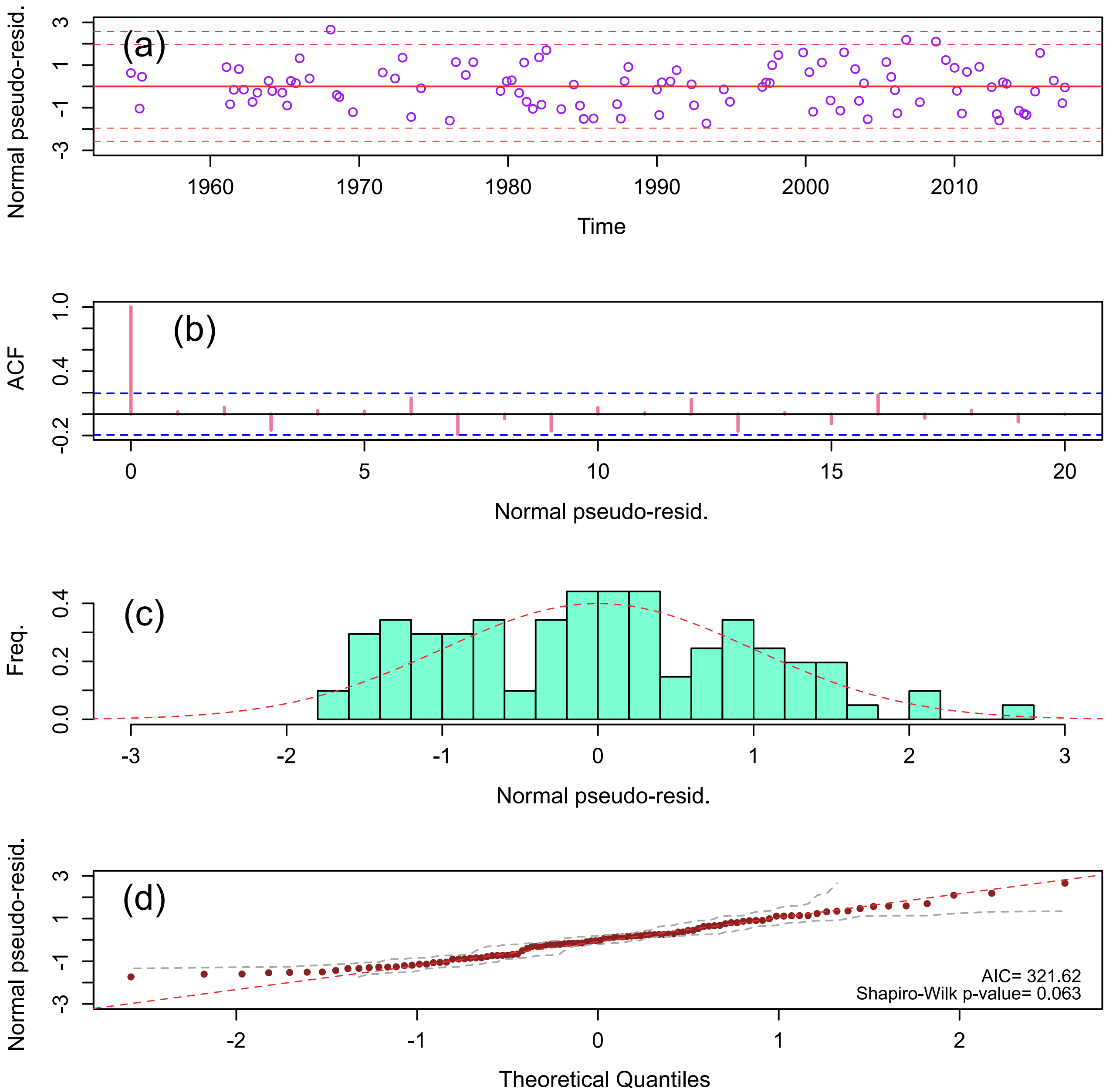

Figure S5: Diagnostic plots of the model residuals corresponding to the duration HMM output as discussed in Figure 7 for station ID 227211. (a) Time series of the normal pseudo-residuals corresponding to the low flow peaks occurring over time (red lines at 0, ±1.96, ±2.58). (b) Auto-correlation of the normal pseudo-residuals, with the blue dotted lines indicating the 95th percentile confidence intervals for uncorrelated series. (c) Histogram of the normal pseudo-residuals, with the red dotted line indicating a standard normal distribution. (d) Quantile-Quantile (Q-Q) plot of the normal pseudo-residuals in relation to the theoretical quantiles.

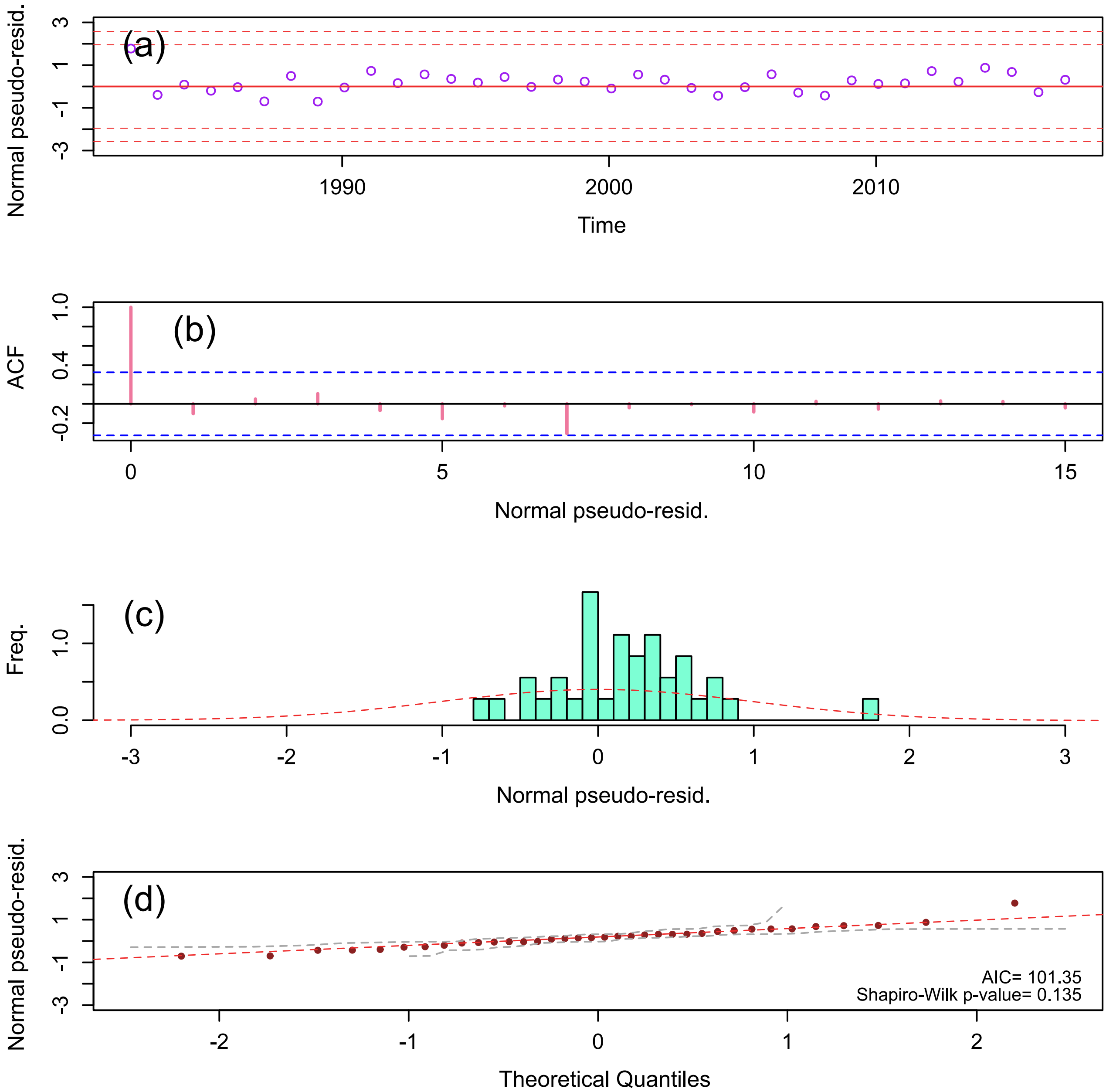

Figure S6: Diagnostics of the model residuals corresponding to the frequency HMM output as discussed in Figure 8 for station ID 227237. Residual (a) Annual time series of the normal pseudo-residuals (red lines at 0, ±1.96, ±2.58). (b) Auto-correlation of the normal pseudo-residuals, with the blue dotted lines indicating the 95th percentile confidence intervals for uncorrelated series. (c) Histogram of the normal pseudo-residuals, with the red dotted line indicating a standard normal distribution. (d) Quantile-Quantile (Q-Q) plot of the normal pseudo-residuals in relation to the theoretical quantiles.

Text S5. Warm periods of ENSO as used in the study

The ONI value at a given month is obtained from a 3-month running mean of the sea surface temperature anomalies of the Niño3.4 region (5°N-5°S, 120-170°W) in the equatorial Pacific Ocean that are above a threshold of 0.5°C. Warm (positive) SST anomalies are associated with El Niño events while La Niña events are typically associated with cold (negative) SST anomalies. Any given value would be considered to be indicating the occurrence of a warm ENSO episode when at least 5 consecutive values in the ONI series lie above the threshold of 0.5°C. The warm periods identified in this way are shown below and are displayed as red vertical strips in Figure 10 of the paper. These were sourced from the United States National Oceanic and Atmospheric Administration (NOAA) Climate Prediction Centre (CPC) (`www.cpc.ncep.noaa.gov`).

Table S3: List of the warm periods of the ONI as used in Figure 10 of the paper.

MJJ 1951	MJJ 1958	AMJ 1969	AMJ 1982	JAS 1991	SON 2002	MJJ 2015
JJA 1951	JJA 1958	JAS 1969	MJJ 1982	ASO 1991	OND 2002	JJA 2015
JAS 1951	OND 1958	ASO 1969	JJA 1982	SON 1991	NDJ 2002	JAS 2015
ASO 1951	NDJ 1958	SON 1969	JAS 1982	OND 1991	DJF 2003	ASO 2015
SON 1951	DJF 1959	OND 1969	ASO 1982	NDJ 1991	JFM 2003	SON 2015
OND 1951	JFM 1959	NDJ 1969	SON 1982	DJF 1992	JJA 2004	OND 2015
NDJ 1951	FMA 1959	DJF 1970	OND 1982	JFM 1992	JAS 2004	NDJ 2015
DJF 1952	MJJ 1963	AMJ 1972	NDJ 1982	FMA 1992	ASO 2004	DJF 2016
JFM 1953	JJA 1963	MJJ 1972	DJF 1983	MAM 1992	SON 2004	JFM 2016
FMA 1953	JAS 1963	JJA 1972	JFM 1983	AMJ 1992	OND 2004	FMA 2016
MAM 1953	ASO 1963	JAS 1972	FMA 1983	MJJ 1992	NDJ 2004	MAM 2016
AMJ 1953	SON 1963	ASO 1972	MAM 1983	ASO 1994	DJF 2005	
MJJ 1953	OND 1963	SON 1972	AMJ 1983	SON 1994	JFM 2005	
JJA 1953	NDJ 1963	OND 1972	MJJ 1983	OND 1994	ASO 2006	
JAS 1953	DJF 1964	NDJ 1972	ASO 1986	NDJ 1994	SON 2006	
ASO 1953	JFM 1964	DJF 1973	SON 1986	DJF 1995	OND 2006	
SON 1953	AMJ 1965	JFM 1973	OND 1986	JFM 1995	NDJ 2006	
OND 1953	MJJ 1965	FMA 1973	NDJ 1986	FMA 1995	DJF 2007	
NDJ 1953	JJA 1965	ASO 1976	DJF 1987	AMJ 1997	JJA 2009	
DJF 1954	JAS 1965	SON 1976	JFM 1987	MJJ 1997	JAS 2009	
JFM 1954	ASO 1965	OND 1976	FMA 1987	JJA 1997	ASO 2009	
MAM 1957	SON 1965	NDJ 1976	MAM 1987	JAS 1997	SON 2009	
AMJ 1957	OND 1965	DJF 1977	AMJ 1987	ASO 1997	OND 2009	
MJJ 1957	NDJ 1965	JFM 1977	MJJ 1987	SON 1997	NDJ 2009	
JJA 1957	DJF 1966	ASO 1977	JJA 1987	OND 1997	DJF 2010	
JAS 1957	JFM 1966	SON 1977	JAS 1987	NDJ 1997	JFM 2010	
ASO 1957	FMA 1966	OND 1977	ASO 1987	DJF 1998	FMA 2010	
SON 1957	MAM 1966	NDJ 1977	SON 1987	JFM 1998	SON 2014	
OND 1957	SON 1968	DJF 1978	OND 1987	FMA 1998	OND 2014	
NDJ 1957	OND 1968	SON 1979	NDJ 1987	MAM 1998	NDJ 2014	
DJF 1958	NDJ 1968	OND 1979	DJF 1988	AMJ 1998	DJF 2015	
JFM 1958	DJF 1969	NDJ 1979	JFM 1988	MJJ 2002	JFM 2015	
FMA 1958	JFM 1969	DJF 1980	AMJ 1991	JJA 2002	FMA 2015	
MAM 1958	FMA 1969	JFM 1980	MJJ 1991	JAS 2002	MAM 2015	
AMJ 1958	MAM 1969	MAM 1982	JJA 1991	ASO 2002	AMJ 2015	

References

Forney, G. D. (1973). The viterbi algorithm. *Proceedings of the IEEE*, *61*(3), 268–278.

Goswami, P., Peterson, T. J., Mondal, A., & Rüdiger, C. (2022). Non-stationary Influences of Large-scale Climate Drivers on Low Flow Extremes in Southeast Australia. *Water Resources Research*, e2021WR031508.

Peterson, T. J., Saft, M., Peel, M. C., & John, A. (2021). Watersheds may not recover from drought. *Science*, *372*(6543), 745–749. doi: 10.1126/science.abd5085

Price, K., Storn, R. M., & Lampinen, J. A. (2006). *Differential evolution: a practical approach to global optimization*. Springer Science & Business Media.

Storn, R., & Price, K. (1997). Differential Evolution - A Simple and Efficient Heuristic for Global Optimization over Continuous Spaces. *Journal of Global Optimization*, *11*(4), 341–359. doi: 10.1023/A:1008202821328

Zucchini, W., & MacDonald, I. L. (2009). *Hidden Markov models for time series: an introduction using R*. Chapman and Hall/CRC.